Robotica (2017) volume 35, pp. 1263–1279. © Cambridge University Press 2016
doi:10.1017/S0263574716000035

Cascaded control for balancing an inverted pendulum on a flying quadrotor

Chao Zhang†‡*, Huosheng Hu‡, Dongbing Gu‡ and Jing Wang†

†*Engineering Research Institute of USTB, University of Science and Technology Beijing, Beijing, China. E-mail: wangj@nercar.ustb.edu.cn*
‡*Department of Computer Science and Electronic Engineering, University of Essex, Colchester, UK. E-mails: hhu@essex.ac.uk, dgu@essex.ac.uk*

(Accepted January 11, 2016. First published online: February 9, 2016)

SUMMARY
This paper is focused on the flying inverted pendulum problem, i.e., how to balance a pendulum on a flying quadrotor. After analyzing the system dynamics, a three loop cascade control strategy is proposed based on active disturbance rejection control (ADRC). Both the pendulum balancing and the trajectory tracking of the flying quadrotor are implemented by using the proposed control strategy. A simulation platform of 3D mechanical systems is deployed to verify the control performance and robustness of the proposed strategy, including a comparison with a Linear Quadratic Controller (LQR). Finally, a real quadrotor is flying with a pendulum to demonstrate the proposed method that can keep the system at equilibrium and show strong robustness against disturbances.

KEYWORDS: Inverted pendulum; Micro aerial vehicles; Active disturbance rejection control; Cascade control.

1. Introduction

The inverted pendulum is a typical non-linear control problem, and has been investigated for several decades. It is also a common benchmark to evaluate advanced control techniques. Recently, it has been extended to many different application scenarios, such as an inverted pendulum on a cart, multi-degree pendulum and Furuta pendulum.[1] The dynamics of these pendulum systems is related to two-wheel robots, rocket guidance, etc,[2] and many advanced control strategies have been deployed, including PID control,[3] neural networks control[4] and controlled Lagrangians method.[5]

With the recent advancement of micro electro mechanical sensors (MEMS) and energy storage devices, Micro Aerial Vehicles (MAVs) have demonstrated a great potential. They have been widely used in many civilian and military applications, e.g., wildfire monitoring, aerial filming and pollution assessment due to their easy construction and ability to takeoff and land vertically (VTOL).[6] Meanwhile, thanks to their simple steering principle and low cost,[7] these small flying machines especially quadrotors are seen in research institutes worldwide, including the Autonomous Systems Lab at Swiss Federal Institute of Technology[8] and the General Robotics, Automation, Sensing and Perception (GRASP) Laboratory at University of Pennsylvania.[9]

Recently, the flying inverted pendulum has attracted a lot of attention. It is a non-linear, under-actuated and coupled system with 8 Degrees of freedom (DOFs), i.e., a 6-DOF quadrotor and a 2-DOF pendulum. ETH Flying Lab is the first in the world to investigate this problem.[10] After the nominal pendulum equilibrium was realized, linear state feedback controllers were designed to stabilize the whole system. Then, reinforcement learning was adopted to improve system performance by dividing the task into two subtasks: initial balancing and balanced hover.[11] In addition, a global stabilizing

* Corresponding author. E-mail: czhangd@essex.ac.uk

controller for inverted pendulum derived from controlled Lagrangians is used, together with another parallel quadrotor position controller to generate attitude commands.[12]

In general, linear state feedback design is based on a linearization model around the equilibrium point. The model is only valid in a small neighborhood and vulnerable to disturbances. Meanwhile, the parameters of two independent controllers for the pendulum and the quadrotor are difficult to tune and need many trials. Although reinforcement learning could be adopted in the controller design by dividing the task into two subtasks, the designed controller actually is not controlling the pendulum and quadrotor positions together. The final quadrotor position may be dozens of meters away from the origin.[11] Some other non-linear control methods,[13] such as controlled Lagrangian method, are very rigorous mathematically for a single inverted pendulum, which are however too complex to be used in systems.

The classic inverted pendulum research may provide some ideas, but is difficult to be directly applied to the flying pendulum system that has an unstable equilibrium, i.e., the upward vertical position of the pendulum. Its internal and external disturbances are ubiquitous and difficult to be described in a mathematical way. Other factors such as communication delay and aerodynamics may degrade the control quality in practical systems as well.[14]

Recently, two disturbance estimation techniques[15] have been proposed for disturbance rejection. One is the disturbance observer technique proposed by Ohnishi *et al.*,[16] which has been widely applied to missile systems,[17] humanoid joint,[18] precise motion control systems.[19] The other is ADRC, which estimates internal and external disturbances online by using an extended state observer (ESO), and then compensates them in control input signals.[20] Since ADRC does not require an accurate mathematical model and is easy to be realized, it has been widely deployed in many practical systems with promising results.[21] A two-loop linear ADRC controller is designed for a classic inverted pendulum on a cart in ref. [22]. It is clear that linear ADRC shows great potential to solve the under-actuated non-linear system control problem.

Inspired by all the previous related work, we propose a three-loop cascade linear ADRC architecture for the flying pendulum system in this paper such that the quadrotor can track its reference trajectory while the inverted pendulum stays at the equilibrium (vertical position). The inner loop is a high bandwidth onboard controller, which tracks desired attitude angles using feedbacks from inertial measurement units (IMU). The quadrotor can respond to the commands fast since it has very low rotational inertia and powerful brushless motors. Therefore, on the basis of the inner loop, an ADRC controller for the pendulum position is designed using the tangent of angles as pseudo control inputs.

In order to design the outer loop controller for quadrotor horizontal positions, the time scale control concept[23] is adopted since the stability of the inverted pendulum has to be guaranteed first and thus position responses of the quadrotor has to be slower. An ADRC controller using the pendulum position as control inputs is adopted here, with smaller parameters to meet the time-scale separation principle. Another independent controller using total thrust as control input is designed for the altitude of the quadrotor. From simulations, we find system performance is sensitive to the gain coefficient of control inputs, thus we introduce an adaptive gain parameter after analyzing the system.

Through this multi-level design, each sub-loop is a negative feedback controller that differs from the common LQR and PID controllers. The vehicle loop is a positive feedback controller. This change can utilize the natural connection between all sub-loops and can improve flying safety in experimental flights. The robustness of the system is validated by adding disturbances during flying. In addition, this system involves many communications such as TCP/IP connection from Vicon system to PC and wireless Zigbee connection from PC to the quadrotor. Time delay is an important issue here and may affect system stability. Inspired by Lupashin's work,[8] we proposed a compensation algorithm to generate estimation feedbacks and velocities, which is simple and effective.

The remainder of this paper is organized as follows. Section 2 presents the dynamics model of the quadrotor-pendulum system used in this research. In Section 3, a cascade linear ADRC controller is designed for quadrotor trajectory tracking and inverted pendulum balancing. Simulation on the Matlab SimMechanics platform[24] and experimental flights are carried out in Section 4 to show the feasibility and effectiveness of the proposed control strategy. Finally, a brief conclusion and future work are given in Section 5.

https://doi.org/10.1017/S0263574716000035 Published online by Cambridge University Press

Fig. 1. Fixed body and world coordinate systems.

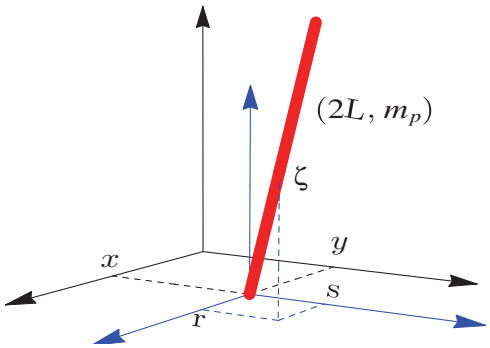

Fig. 2. Inverted pendulum on top of a quadrotor.

2. System Dynamics

A Humming bird quadrotor made by Ascending Technology is adopted in this research.[25] Two right-handed coordinate systems used for describing the MAV pose is shown in Fig. 1. The world frame, $\mathcal{W}$, is defined by axes X_W,Y_W and Z_W with Z_W axis pointing upward. The body frame, $\mathcal{B}$, coincides with the center of mass and is defined by the axes X_B,Y_B and Z_B. X_B is always aligned with the preferred forward direction and Z_B perpendicular to the plane of four rotors. To simplify the analysis, some reasonable assumptions are given here without loss of generality.

Assumption 1. The body-fixed frame $\mathcal{B}$ is attached to the center of mass of the quadrotor and the pendulum is rigidly attached to the center as well.

Assumption 2. The z position of the quadrotor can be well controlled and is nearly fixed.

Assumption 3. Dynamics of the quadrotor is not affected by the movements of the pendulum since the mass and the inertia of the pendulum are one magnitude less than that of the quadrotor.

2.1. Quadrotor-pendulum model

As shown in Fig. 2, the position vector of the quadrotor is denoted by $\mathbf{p} = [x\ y\ z]^T$ in the world frame and the pendulum position is described by $\mathbf{p_r} = [r\ s\ \zeta]^T$, which represents the translational position of the pendulum mass center relative to the supporting point, i.e., r along the X_W-axis, s along the Y_W-axis and ζ the Z_W-axis. The relative height ζ can be calculated by $\sqrt{L^2 - r^2 - s^2}$, where L is the length from the pendulum bottom to the mass center. Thus, the pendulum position with respect to $\mathcal{W}$ can be given by $\mathbf{p}_p = [x + r\ y + s\ z + \zeta]^T$.

Since the pendulum has no moment of inertia about its z-axis, its rotation kinetic energy can be given by $\frac{1}{6} m_p L^2 \Omega_{p,xy}^T \Omega_{p,xy}$ where m_p is the pendulum mass and $\Omega_{p,xy}$ is the angular rate. From

https://doi.org/10.1017/S0263574716000035 Published online by Cambridge University Press

the rigid body kinematics, we can derive $\Omega_{p,xy} = \mathbf{p}_r \times \dot{\mathbf{p}}_r / L^2$. The total kinetic energy T_p and the potential energy V_p of the pendulum are

$$T_p = \frac{1}{2} m_p \left((\dot{x} + \dot{r})^2 + (\dot{y} + \dot{s})^2 + \left(\dot{z} - \frac{r\dot{r} + s\dot{s}}{\zeta} \right)^2 \right) + \frac{1}{6} m_p L^2 \Omega_{p,xy}^T \Omega_{p,xy}, \tag{1}$$

$$V_p = m_p g (z + \zeta). \tag{2}$$

To derive the pendulum dynamics, Lagrangian mechanics is applied as below:

$$\frac{d}{dt} \left(\frac{\partial L_p}{\partial (\dot{r}, \dot{s})} \right) - \frac{\partial L_p}{\partial (r, s)} = 0, \tag{3}$$

where $L_p = T_p - V_p$. Then, we obtain

$$\begin{aligned} \ddot{r} = & -\frac{3}{4} \left(\frac{\zeta^2}{L^2 - s^2} \right) \ddot{x} + \frac{3r\zeta(g + \ddot{z})}{4(L^2 - s^2)} \\ & + \frac{r^3(\dot{s}^2 + s\ddot{s}) - 2r^2 s\dot{r}\dot{s} + r(-L^2 s\ddot{s} + s^3\ddot{s} + s^2\dot{r}^2 - L^2\dot{r}^2 - L^2\dot{s}^2)}{(L^2 - s^2)\zeta^2}, \end{aligned} \tag{4}$$

$$\begin{aligned} \ddot{s} = & -\frac{3}{4} \left(\frac{\zeta^2}{L^2 - r^2} \right) \ddot{y} + \frac{3s\zeta(g + \ddot{z})}{4(L^2 - r^2)} \\ & + \frac{s^3(\dot{r}^2 + r\ddot{r}) - 2s^2 r\dot{s}\dot{r} + s(-L^2 r\ddot{r} + r^3\ddot{r} + r^2\dot{s}^2 - L^2\dot{s}^2 - L^2\dot{r}^2)}{(L^2 - r^2)\zeta^2}. \end{aligned} \tag{5}$$

From the dynamic equations, the accelerations can be regarded as control inputs to the system. $\ddot{z}$ is always small and considering the gain coefficient of $\ddot{z}$ is also much smaller than those of $\ddot{x}$ and $\ddot{y}$, it can be handled as an internal disturbance to the pendulum. So the system dynamics of the pendulum can be written in the following form:

$$[\ddot{r}\ \ddot{s}]^T = B[\ddot{x}\ \ddot{y}]^T + \mathbf{f_z}(r, s)\ddot{z} + \mathbf{f_n}(r, s, \dot{r}, \dot{s}), \tag{6}$$

where $\mathbf{f_z}$ and $\mathbf{f_n}$ are the second term and third term of the right-hand sides of Eqs. (4) and (5) respectively, and

$$B = \begin{bmatrix} -\frac{3}{4} \left(\frac{\zeta^2}{L^2 - s^2} \right) & 0 \\ -\frac{3}{4} \left(\frac{\zeta^2}{L^2 - r^2} \right) & 0 \end{bmatrix}. \tag{7}$$

2.2. Quadrotor dynamics

The quadrotor pose is described in 6 DOF: the translational position in the world frame and the vehicle attitude parameterized by XYZ-Euler angles (roll-ϕ,pitch-θ,yaw-ψ). Using the Newton's second law, translational equations of the MAV motion can be derived as below:.[26]

$$m\ddot{\mathbf{p}} = \begin{bmatrix} 0 \\ 0 \\ -mg \end{bmatrix} + R \begin{bmatrix} 0 \\ 0 \\ T \end{bmatrix}, \tag{8}$$

where R is the rotational matrix of body frame with respect to the world frame, m, g denote the total mass and the gravitational constant respectively and T is the total thrust produced by four propellers.

https://doi.org/10.1017/S0263574716000035 Published online by Cambridge University Press

The attitude is not directly controllable, but R is related to the angular velocity of the quadrotor in the body frame, which can be described by the following equation:

$$\dot{R} = R\hat{\Omega}, \tag{9}$$

where $\Omega = [w_x, w_y, w_z]^{\mathrm{T}}$ denotes the angular velocity vector w.r.t $\mathcal{B}$. The notation $\hat{\Omega}$ is the skew-symmetric matrix of Ω. And the angular acceleration is determined by torques generated by four propellers.

$$J\dot{\Omega} = -\Omega \times J\Omega + \tau, \tag{10}$$

where J denotes the inertia matrix w.r.t the frame $\mathcal{B}$. The control input $\tau = [\tau_1\ \tau_2\ \tau_3]^T$ represents torques produced by propellers.

Based on these dynamic equations, we have made a high-bandwidth controller to track the desired attitude Euler angle values and in order to transfer these commands to motor speeds, a brief motor model is introduced here. As seen in Fig. 1, motor 1 is the motor on the $+X_B$ arm and the other three motors are allocated to $+Y_B$, $-X_B$, $-Y_B$ arms, respectively. For a typical multi-rotor flying vehicle, each rotor produces a thrust force F_i in its Z_B-axis and a torque M_i around its Z_B-axis. A basic relationship between them and motor rotation speed n_i is $F_i = k_f n_i^2$, $M_i = k_m n_i^2$. The parameters k_f and k_m can be regarded as constants and be determined from static thrust tests. Then, we can write the general relationship in a matrix form for the quadrotor used in this paper.

$$\begin{bmatrix} \tau_1 \\ \tau_2 \\ \tau_3 \\ T \end{bmatrix} = \begin{bmatrix} 0 & lk_f & 0 & -lk_f \\ -lk_f & 0 & lk_f & 0 \\ k_m & -k_m & k_m & -k_m \\ k_f & k_f & k_f & k_f \end{bmatrix} \begin{bmatrix} n_1^2 \\ n_2^2 \\ n_3^2 \\ n_4^2 \end{bmatrix}, \tag{11}$$

where l denotes the distance from rotor to the center of quadrotor, and the unit of motor speed is revolutions per minute (rpm). Hence, we can achieve the required motor speeds by inverse operation of Eq. (11). The attitude control loop and the calculation of the motor speed run on the Asctec Autopilot board mounted on the quadrotor at 1 KHz.

3. Controller Design

The quadrotor-pendulum control system includes three loops, i.e., the onboard attitude loop based on IMU feedbacks, the pendulum balancing loop and the quadrotor position loop. Since the system is underactuated and the vertical position of the pendulum is an unstable equilibrium, a cascade control strategy is adopted, i.e., the middle loop is the pendulum control and the quadrotor position loop is the outer loop. Desired attitude angles and thrust are tracked by onboard inner loop. The overall system structure can be seen in Fig. 3.

3.1. Inverted pendulum loop

The target of the middle loop is to keep the pendulum staying at the equilibrium point, i.e., $r, s \approx 0$. From Eq. (8), we can derive

$$\begin{aligned} \ddot{x} &= (\sin\psi \sin\phi + \cos\psi \sin\theta \cos\phi)T/m, \\ \ddot{y} &= (-\cos\psi \sin\phi + \sin\psi \sin\theta \cos\phi)T/m, \\ \ddot{z} &= (\cos\theta \cos\phi)T/m - g. \end{aligned} \tag{12}$$

https://doi.org/10.1017/S0263574716000035 Published online by Cambridge University Press

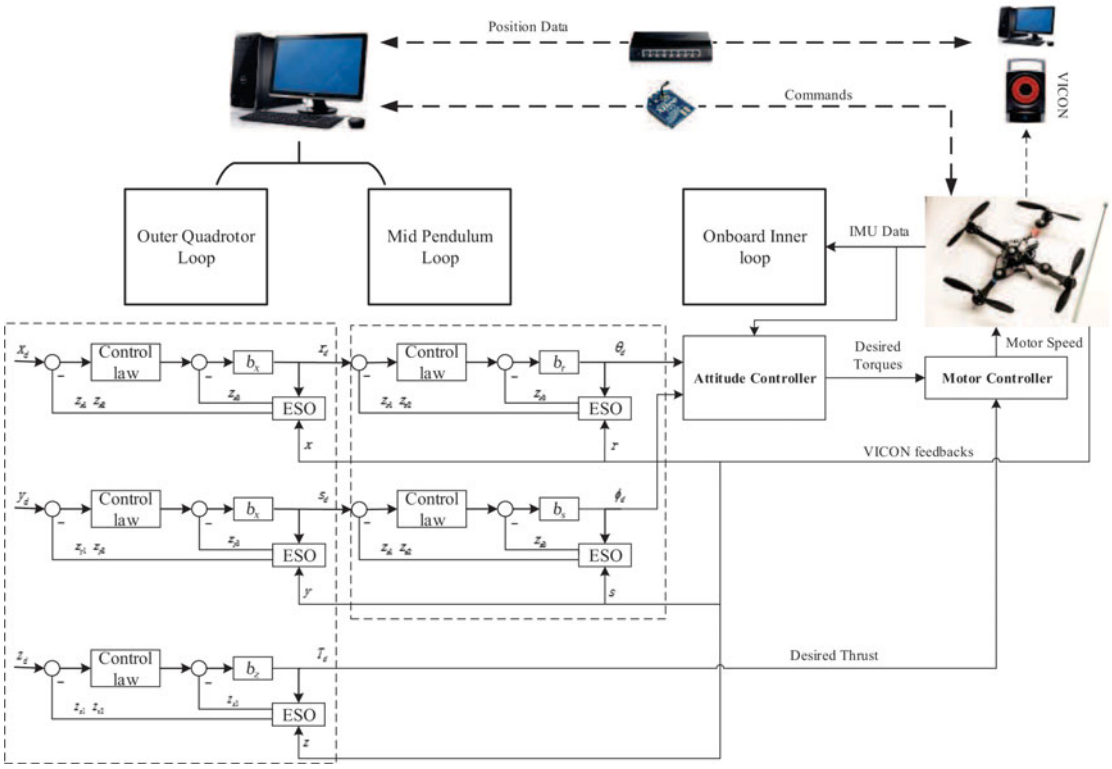

Fig. 3. An overview of the experimental flying pendulum system.

For simplification, it is assumed that the yaw angle is always kept near zero. Substitute Eq. (12) into Eq. (6) and take the attitude angles as control inputs

$$\ddot{r} = -\frac{3}{4}\left(1 - \frac{r^2}{L^2 - s^2}\right) g \tan\theta + f_r, \tag{13}$$

$$\ddot{s} = \frac{3}{4\cos\theta}\left(1 - \frac{s^2}{L^2 - r^2}\right) g \tan\phi + f_s, \tag{14}$$

where f_r represents the non-linear dynamics produced by $\ddot{z}$, s, r and parameter uncertainties, and f_s represents external disturbances.

Linear ADRC control is adopted here to handle complex disturbance compensation. Take the r-$\tan\theta$ loop as an example to show more details. A linear ESO with the following discrete form is employed to estimate the system states $[r\ \dot{r}\ f_r]^T$ including the extended state f_r.

$$\begin{cases} e_r = z_{r1} - \hat{r} \\ b_r = -\dfrac{3}{4}\left(1 - \dfrac{r^2}{L^2 - s^2}\right) g \\ z_{r1} = z_{r1} + h(z_{r2} - \beta_{r1} e_r) \\ z_{r2} = z_{r2} + h(z_{r3} - \beta_{r2} e_r + b_r \tan\theta) \\ z_{r3} = z_{r3} + h(-\beta_{r3} e_r) \end{cases}, \tag{15}$$

where $\hat{r}$ denotes the measurement value of r, e_r is the tracking error, $z_{ri}(i = 1, 2, 3)$ represents outputs of the ESO, h is the sampling time and $\beta_{ri}(i = 1, 2, 3)$ is observer gains to be tuned. Generally, the larger the observer gain is, the faster response and better performance the system will have. However, a large gain will increase noise sensitivity. According to ref. [27], a proper parameter can be acquired,

https://doi.org/10.1017/S0263574716000035 Published online by Cambridge University Press

which can achieve a compromise between the suppression performance and the noise tolerance in experimental practical system tuning.

Through the ESO, observations of position, velocity and unknown lumped uncertainties are achieved. Hence, the state error feedback control law is designed as follows:

$$u_r = (k_{rp}(r_d - z_{r1}) - k_{rd}(z_{r2}) - z_{r3})/b_r, \tag{16}$$

where u_r is $\tan\theta$ here, k_{rp}, k_{rd} are the controller gains and r_d is the reference command for the outer loop.

The controller and observer of the $s - \tan\phi$ loop can be derived in the same way.

$$\begin{cases} e_s = z_{s1} - \hat{s} \\ b_s = \dfrac{3}{4\cos\theta}\left(1 - \dfrac{s^2}{L^2 - r^2}\right) g \\ z_{s1} = z_{s1} + h(z_{s2} - \beta_{s1} e_s) \\ z_{s2} = z_{s2} + h(z_{s3} - \beta_{s2} e_s + b_s \tan\phi) \\ z_{s3} = z_{s3} + h(-\beta_{s3} e_s) \end{cases} \tag{17}$$

$$u_s = (k_{sp}(s_d - z_{s1}) - k_{sd}(z_{s2}) - z_{s3})/b_s. \tag{18}$$

All the variables have the same definitions as those in Eqs. (15) and (16). The desired angle commands for the onboard attitude loop can be achieved by anti-tangent calculation.

$$\theta_d = \arctan u_r, \ \phi_d = \arctan u_s. \tag{19}$$

3.2. Quadrotor position loop

In order to stabilize the inverted pendulum when the quadrotor is moving, a fast response speed of the middle loop has to be guaranteed and the quadrotor position loop has to be relatively slow. So it is reasonable to assume that the variables r, s are in a steady state due to this time scale separation. The MAV reference trajectories $p_d = [x_d(t),\ y_d(t),\ z_d(t)]^T$ are generated with sufficient smoothness and bounded time derivatives. The altitude of the quadrotor is controlled by an independent ADRC controller. Therefore, the outer loop controller is actually $x - r$ and $y - s$ loops. From Eqs. (13)–(16), by defining external disturbances and unmodeled dynamics together as ξ_x and ξ_y, we can derive

$$\begin{cases} \ddot{x} = b_x r + f_x \\ \ddot{y} = b_y s + f_y \end{cases}, \tag{20}$$

where b_x, b_y are the estimated control input gains and f_x, f_y stand for the whole non-linear dynamics and disturbances

$$\begin{cases} b_x = -\dfrac{g}{\zeta} \\ b_y = -\dfrac{g}{\zeta} \\ f_x = \dfrac{-4(r^3(\dot{s}^2 + s\ddot{s}) - 2r^2 s\dot{r}\dot{s} + r(-L^2 s\ddot{s} + s^3\ddot{s} + s^2\dot{r}^2 - L^2\dot{r}^2 - L^2\dot{s}^2))}{3\zeta^4} + \xi_x \\ f_y = \dfrac{-4(s^3(\dot{r}^2 + s\ddot{r}) - 2s^2 r\dot{s}\dot{r} + s(-L^2 r\ddot{r} + r^3\ddot{r} + r^2\dot{s}^2 - L^2\dot{s}^2 - L^2\dot{r}^2))}{3\zeta^4} + \xi_y. \end{cases} \tag{21}$$

https://doi.org/10.1017/S0263574716000035 Published online by Cambridge University Press

The design of the outer linear ADRC controller is similar to that of the pendulum loop, hence the details are omitted and the results are shown as follows:

$$\begin{cases} e_x = z_{x1} - \hat{x} \\ z_{x1} = z_{x1} + h(z_{x2} - \beta_{x1} e_x) \\ z_{x2} = z_{x2} + h(z_{x3} - \beta_{x2} e_x + b_x r_d) \\ z_{x3} = z_{x3} + h(-\beta_{x3} e_x) \\ r_d = (k_{xp}(x_d - z_{x1}) + k_{xd}(\dot{x_d} - z_{x2}) - z_{x3})/b_x \end{cases} \tag{22}$$

$$\begin{cases} e_y = z_{y1} - \hat{y} \\ z_{y1} = z_{y1} + h(z_{y2} - \beta_{y1} e_y) \\ z_{y2} = z_{y2} + h(z_{y3} - \beta_{y2} e_y + b_y s_d) \\ z_{y3} = z_{y3} + h(-\beta_{y3} e_y) \\ s_d = (k_{yp}(y_d - z_{y1}) + k_{yd}(\dot{y_d} - z_{y2}) - z_{y3})/b_y \end{cases} . \tag{23}$$

It is worth noting that the control parameters in the outer loop have to be much smaller than those in the middle loop to implement the two-time-scale control.

3.3. Time delay compensation

In the experimental system, the famous motion capture system VICON is deployed to measure the position of the quadrotor and the pendulum. A commercial computer will acquire these data through TCP/IP and send commands to the onboard controller via wireless Zigbee modules. System latency is caused mainly by communications. If the pendulum has made a big displacement during the time delay, the vehicle needs a very large acceleration to stabilize the pendulum. However, the maximal acceleration is around 13.1 m/s^2 on Humming bird, and our VICON area has a limited range as well. Therefore, a short delay may result in the pendulum falling down from the quadrotor.

In this paper, a tracking differentiator (TD) is introduced to compensate for system latency on the basis of ESO. The TD input is the raw measurement $\mathbf{y}$ and the outputs are filtered measurement $\tilde{\mathbf{y}}$ and estimated differentiation $\dot{\tilde{\mathbf{y}}}$. The specific TD system is shown as below:

$$\begin{cases} \text{fh} = \text{fhan}(\tilde{\mathbf{y}} - \mathbf{y}, \dot{\tilde{\mathbf{y}}}, r_0, h_0) \\ \tilde{\mathbf{y}} = \tilde{\mathbf{y}} + h\dot{\tilde{\mathbf{y}}} \\ \dot{\tilde{\mathbf{y}}} = \dot{\tilde{\mathbf{y}}} + h\text{fh}, \end{cases} \tag{24}$$

where $\text{fhan}(x_1, x_2, r_0, h_0)$ is a special non-linear function with the following form which can fast track the signal differential.

$$\begin{cases} d = r_0 h_0, d_0 = h_0 d, y = x_1 + h_0 x_2 \\ a_0 = \sqrt{d^2 + 8r_0|y|} \\ a = \begin{cases} x_2 + \dfrac{a_0 - d}{2}\text{sign}(y), & |y| > d_0 \\ x_2 + \dfrac{y}{h_0}, & |y| \le d_0 \end{cases} \\ \text{fhan} = -\begin{cases} r_0 \text{sign}(a), & |a| > d \\ r_0 \dfrac{a}{d}, & |a| \le d \end{cases} , \end{cases} \tag{25}$$

https://doi.org/10.1017/S0263574716000035 Published online by Cambridge University Press

where r_0 and h_0 are positive parameters to determine the tracking speed and the filtering performance, respectively. According to the TD output signals, we can adopt a conventional algorithm to predict the latency-compensated measurements $\hat{\mathbf{y}}$.

$$\hat{\mathbf{y}} = \tilde{\mathbf{y}} + \hat{\tau}\tilde{\dot{\mathbf{y}}}, \tag{26}$$

where $\hat{\tau}$ is the estimated real latency. $\hat{\mathbf{y}}$ is the input of ESO instead of directly measurement $\mathbf{y}$ and the latency-free control is generated using compensated signals. The whole time delay is 30 ms∼50 ms according to experimental test results. We choose $\hat{\tau} = 40$ ms in our controller design.

4. Verification Tests

4.1. Simulation results

To make simulations as accurate as possible, a multibody simulation environment for 3D mechanical systems called SimMechianics on Matlab platform is used instead of numerical equations. The multibody system can be modeled using blocks representing bodies, joints, constraints and force elements, and then SimMechanics formulates and solves the equations of motion for the complete mechanical system. Models in CAD files, including mass, inertia, joint, constraint and 3D geometry, can be imported into SimMechanics and an assembly file with experimental data from the quadrotor and pendulum drawn using Solid works is used in this paper.

Additionally, an automatically generated 3D animation can visualize the system dynamics as shown in Fig. 1. The inner onboard attitude loop consists of three individual PD controllers which show fast response and strong robustness with well-tuned parameters. The controller details are omitted here since they have been mentioned in many papers and works.[25,28] The altitude controller is an independent linear ADRC controller similar to the outer position loop to command the thrust. The higher-level loops, i.e., quadrotor position and pendulum position loops, are running at 50 Hz and 100 Hz respectively, which are the same settings as our experimental system.

First, the simulation for set point tracking is conducted while the pendulum is being balanced. The quadrotor takes off and hovers in first 0–5 s, then a move command is sent to the quadrotor at $t = 5$ s, and a 5 N force disturbance with 0.01 s duration is given to the pendulum at $t = 20$ s. To show the advantage of the proposed method, the results of a LQR controller are illustrated here to compare system performance.

LQR is an efficient method to solve inverted pendulum problems. It has been used for classical pendulum on a cart case[29] and as well as the flying pendulum.[10] To design the LQR controller for the pendulum on a quadrotor system, a linearization has to be done first. Using system state $[r\ \dot{r}\ s\ \dot{s}\ x\ \dot{x}\ y\ \dot{y}]^T$, dynamic equations can be written in the following form by linearizing around the equilibrium point:

$$\begin{cases} \ddot{r} = \dfrac{3g}{4L}r - \dfrac{3}{4}g\tan\theta \\ \ddot{s} = \dfrac{3g}{4L}s + \dfrac{3}{4}g\tan\phi \\ \ddot{x} = g\tan\theta \\ \ddot{y} = -g\tan\phi \end{cases}. \tag{27}$$

Regarding $[\tan\theta\ \ -\tan\phi]$ as control input, the LQR controller can be achieved by a proper selection of matrix Q and R. After many trials, $Q = diag([10;0;10;0;1;0;1;0])$ and $R = diag([1;1])$ are selected and feedback matrix K can be derived. It shows excellent performance on the linear model, however the performance degrades significantly on the non-linear system and we have to tune the feedback gains manually again.

The simulation outputs are shown from Figs. 4 to 7, the left-hand panels are from the proposed controller and the right-hand panels from the LQR controller. On the other hand, LQR actually consists of two parallel controllers and the gains of the vehicle loop are positive,i.e., [1 1.9588] in this case. It means the vehicle position loop is a positive feedback control which is the same as when using

https://doi.org/10.1017/S0263574716000035 Published online by Cambridge University Press

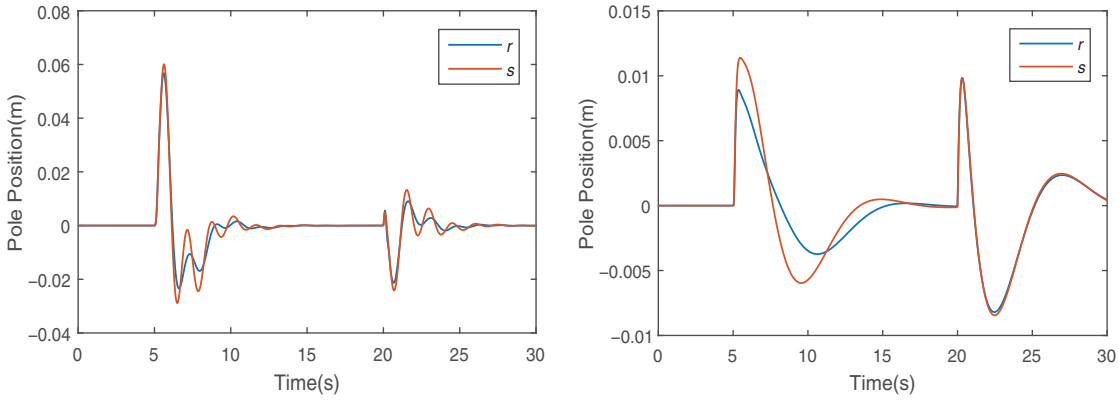

Fig. 4. Pendulum relative position output. (a) Output of the proposed method. (b) Output of the LQR controller.

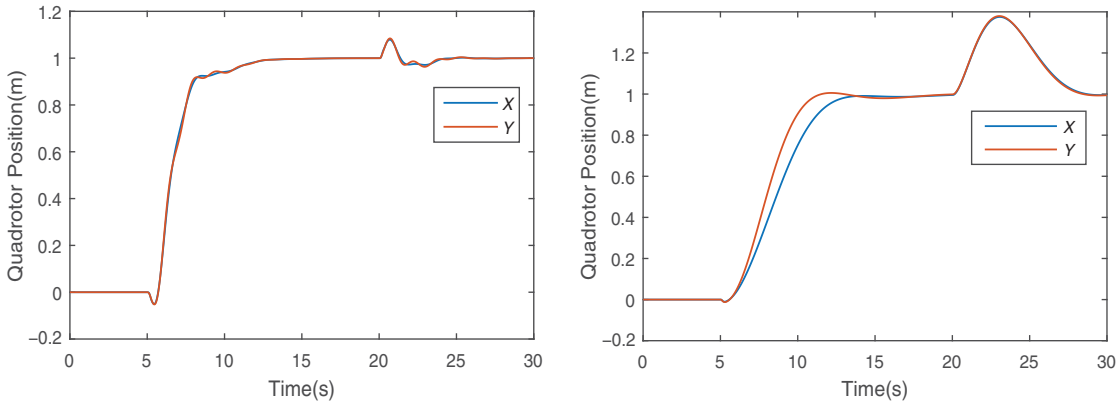

Fig. 5. Quadrotor position output. (a) Output of the proposed method. (b) Output of the LQR controller.

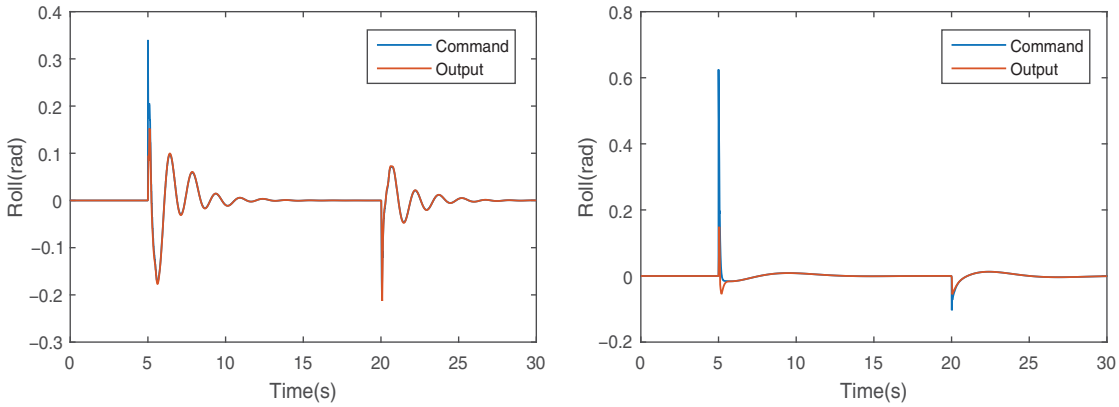

Fig. 6. Roll angle command and output. (a) Output of the proposed method. (b) Output of the LQR controller.

PID controller.[3] The positive feedback will make parameters tuning more complicated and may lose control of the vehicle when being used in experimental flights. LQR needs system state information to build the feedback loop. However, neither the velocities of the vehicle nor the pendulum can be measured directly. Therefore, extra sensors or observer design is needed. But in the proposed control strategy, it is perfectly solved by the ESO design.

Another big difference is the control weight of the pendulum state has to be much greater than that of the quadrotor position state in matrix Q. It is difficult to find a balance between all system states and make the system a good performance on quadrotor position control especially in trajectory tracking. From Figs. 4 and 5, we can see although the pendulum is moving in a smaller range under

https://doi.org/10.1017/S0263574716000035 Published online by Cambridge University Press

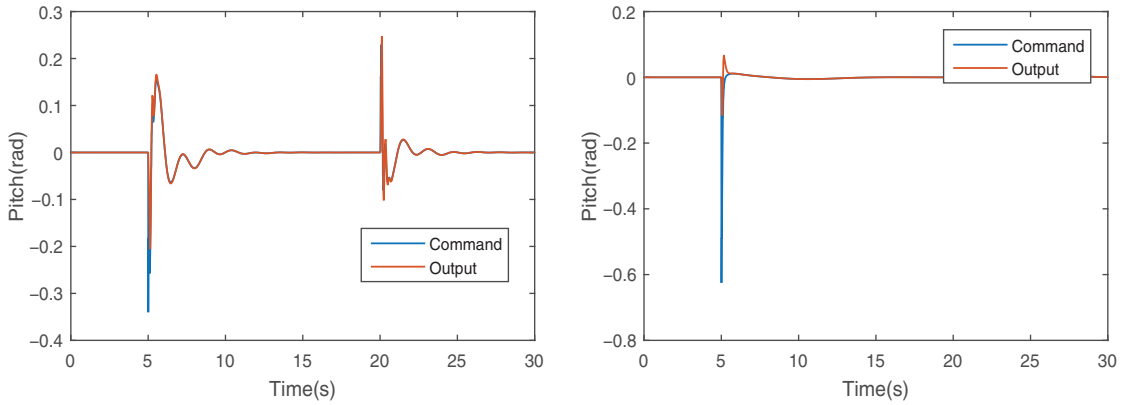

Fig. 7. Pitch angle command and output. (a) Output of the proposed method. (b) Output of the LQR controller.

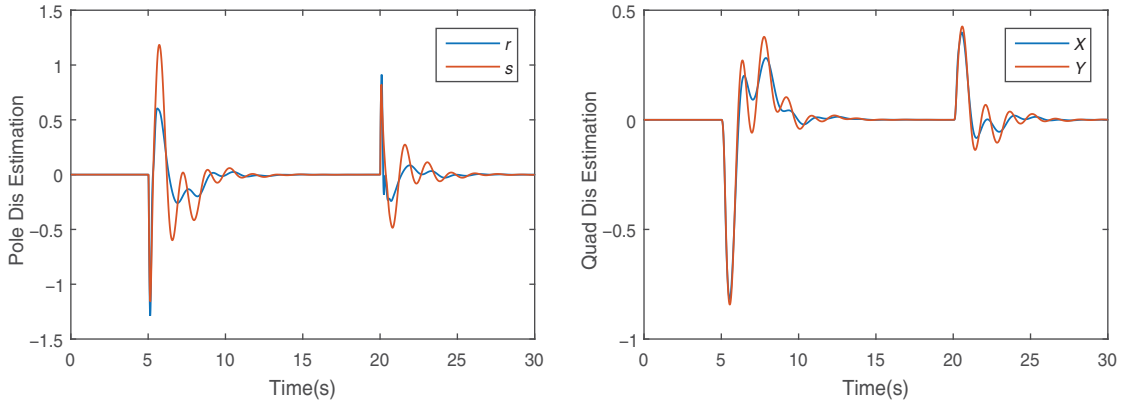

Fig. 8. Disturbance estimation results of system. (a) Estimation output of the middle loop. (b) Estimation output of the outer loop.

the LQR controller, the quadrotor position tracking performance is much worse which takes nearly 10 s to arrive at the set point. This problem can also be solved in the proposed controller since the real-time estimation of the disturbance can cover the functions of the Integral part in PID control and ESO can balance the control input between two loops. Thus, both stable hovering and path tracking can be realized.

On the other hand, the proposed cascade controller behaves more robustly than the LQR, which has shorter reaction time to the disturbance and recovers faster, i.e., 10% versus 40% in displacement and 5 s versus 10 s in recover time. From the angle commands in Figs. 6 and 7, we can also find the system behavior is more aggressive under the proposed method.

The disturbance estimation outputs are shown in Fig. 8. We can see the observer responses rapidly when an external force is exerted. Take the pendulum r position loop for example to show the efficiency clearly, the unmodeled dynamics f_r is calculated with the description in Eq. (4). The comparison between it and the estimated disturbance is shown in Fig. 9. From the figure, we can find the observer estimates the internal dynamic well. We can see the estimation curve does not always coincide with the calculated dynamic curve. It is because that although we have tried our best to build an accurate model for the system, some other factors may still affect the system. For example, the yaw angle cannot always stay at 0 and the quadrotor is not a mass point actually. All the factors will have an influence which can be described on the SimMechanics simulation platform. So it is reasonable that the estimated output is always a little larger than we calculated especially during the adjusting process.

Second, a circular trajectory tracking test of the quadrotor is conducted. The reference trajectory is a circle with 1 m radius. The external disturbance is the same as that in the previous simulation which is exerted at $t = 20$ s. From the results in Figs. 10 and 11, we can see the trajectory tracking of the quadrotor while the pendulum is being balanced can be fulfilled by the proposed controller even

https://doi.org/10.1017/S0263574716000035 Published online by Cambridge University Press

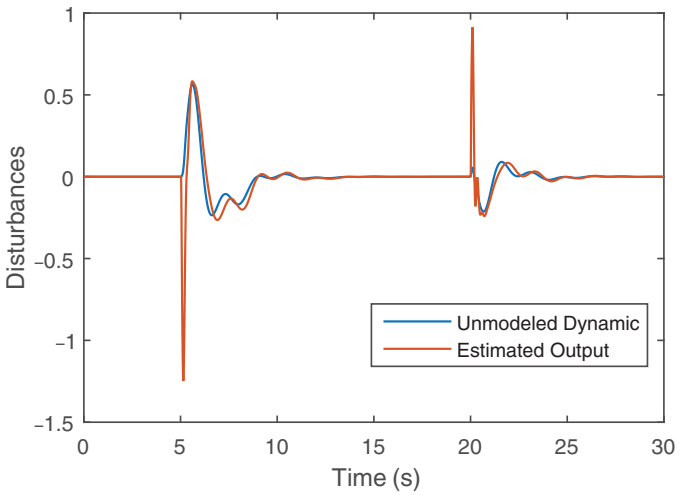

Fig. 9. Comparison of calculated unmodeled dynamic and estimated disturbance output.

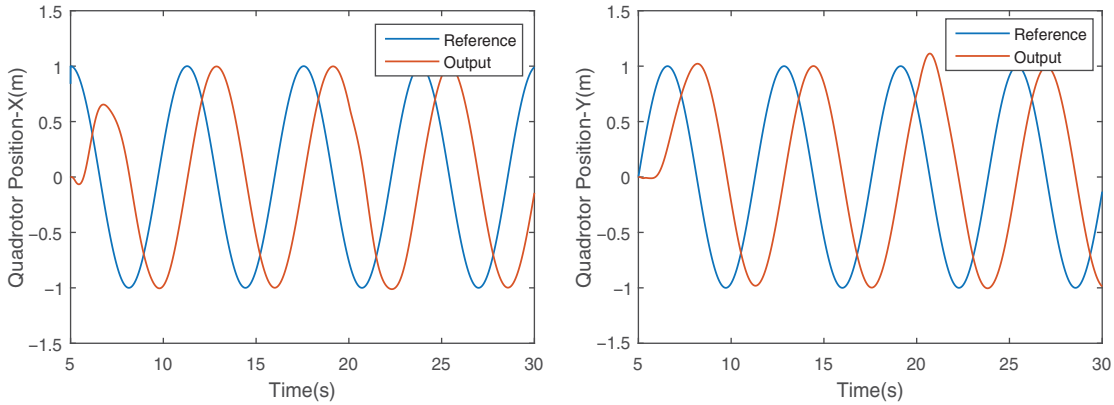

Fig. 10. Reference trajectory tracking outputs of quadrotor. (a) Tracking output in X-axis. (b) Tracking output in Y-axis.

when disturbances exist. The attitude angles are shown in Fig. 12. From the results, we can find it is unnecessary to calculate the accurate pendulum trajectory which was calculated in ref. [10]. The cascade controller can find it itself, i.e., a small circle (see Fig. 11).

4.2. Experimental results

4.2.1. Experiment setup. The proposed control method was implemented in Lab Arena at our university. The vehicle is a Humming bird quadrotor with a spherical universal joint attached to the top. A carbon fiber tube with only light weight is used as the inverted pendulum. The joint base is approximately 7 cm above the quadrotor geometrical center and is 0.39 m away from the pendulum mass center. Figure 3 shows the whole flying pendulum system architecture and the experimental system's specific parameters are shown in Table I. A pair of wireless Zigbee modules are used to exchange data between the onboard attitude controller and the higher level control algorithms at a frequency of 50 Hz. The Vicon system is running at 100 Hz and communicates with our conventional desktop via a gigabit ethernet. Figure 13 shows the quadrotor is hovering while the inverted pendulum is being balanced.

4.2.2. Experiments and analysis. Balancing and hovering is tested at first. The quadrotor is hovering without balancing control in the beginning and will switch to the cascade controller when the pendulum relative horizonal position (r, s) is smaller than 3 cm. The results are shown in Figs. 14 and 15. The cascade controller is switched on at approximately $t = 5$ s. The positions of the pendulum and the quadrotor converge to zero at approximately $t = 11.8$ s. After the system becomes stable,

https://doi.org/10.1017/S0263574716000035 Published online by Cambridge University Press

Table I. Parameters of the experimental system.

Symbol	Definition	Value	Unit
m	Mass of quad	0.55	Kg
m_p	Mass of pendulum	13.5	g
L	Half length of pendulum	0.39	m
l	Arm Length of quad	0.17	m
J_{xx}	Moment of inertia in x	0.0023	Kg m^2
J_{yy}	Moment of inertia in y	0.0028	Kg m^2
J_{zz}	Moment of inertia in z	0.0046	Kg m^2
k_f	Thrust coefficient	5.9×10^{-8}	N/rpm^2
k_m	Moment coefficient	1.3×10^{-9}	Nm/rpm^2

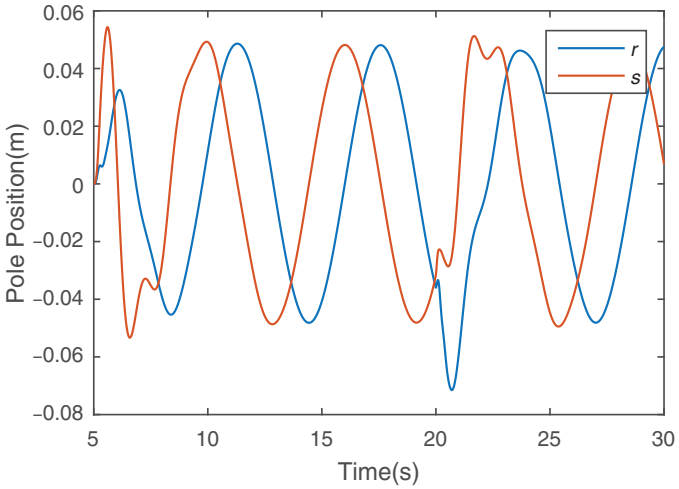

Fig. 11. Pendulum relative position output when moving circles.

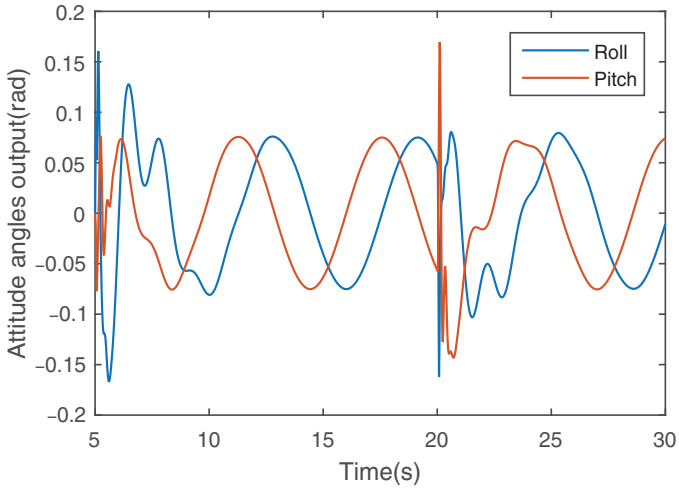

Fig. 12. Quadrotor attitude angles output when moving circles.

external disturbances are given twice by knocking the pendulum with a stick. From the figures, the two knocks can be found at $t \approx 60$ s and $t \approx 75$ s, respectively and the system recovered to the stable state quickly. The average performance is shown in Table II.

Then, a reference trajectory is given to the vehicle. The system is switched to the cascade controller at approximately $t = 7.1$ s, starts hovering at $[0\ 0\ 800]^T$, then goes to the setpoint $[1000\ 0\ 800]^T$ at $t = 65.4$ s, begins to move in a circle at $t = 78.8$ s and back to the origin in the end. The quadrotor

https://doi.org/10.1017/S0263574716000035 Published online by Cambridge University Press

Table II. Results of 10 trials for hovering flights.(MAE is short for maximal absolute error, $S.D.$ is short for standard deviation).

	Settling time(s)	X-MAE(mm)	Y-MAE(mm)	r-MAE(mm)	s-MAE(mm)
$Mean$	7.53	41.31	47.64	27.9883	33.76
$S.D.$	0.9709	9.1414	10.4278	4.6202	4.3345

Fig. 13. An inverted pendulum on a hovering quadrotor.

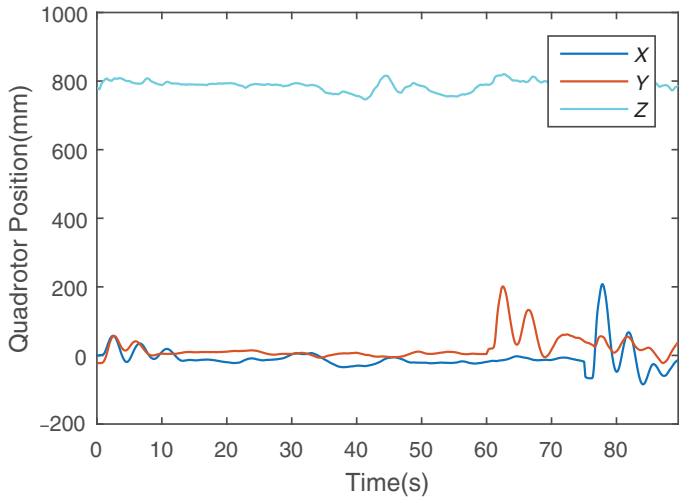

Fig. 14. Quadrotor positions in experimental hovering.

position output is shown in Fig. 16. Figure 17 depicts the pendulum dynamics in flight. Additionally, an experimental flight by the same controller without latency compensation is done here. From outputs comparison shown in Fig. 18, we can find the proposed method works effectively and the output trajectory is more accurate.

From the output comparisons between experiments and simulations, it is clear that the actual response chatters much more heavily and needs longer adjust time. It is because that although we have tried our best to build an accurate mechanical model from a CAD file, it still cannot describe the

https://doi.org/10.1017/S0263574716000035 Published online by Cambridge University Press

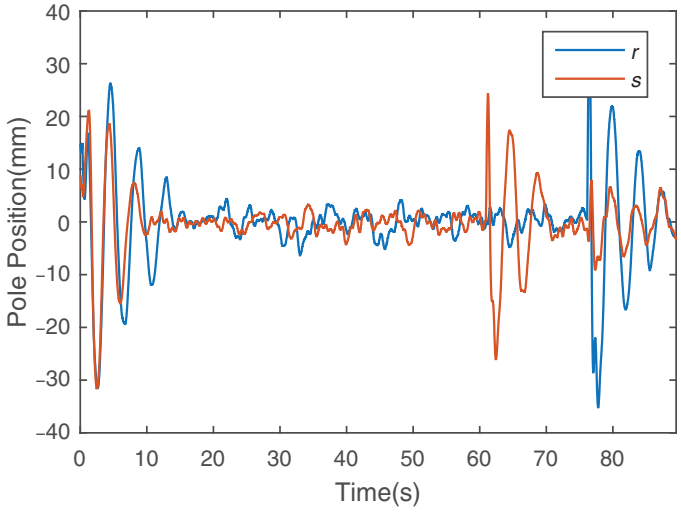

Fig. 15. Pendulum relative position in experimental hovering.

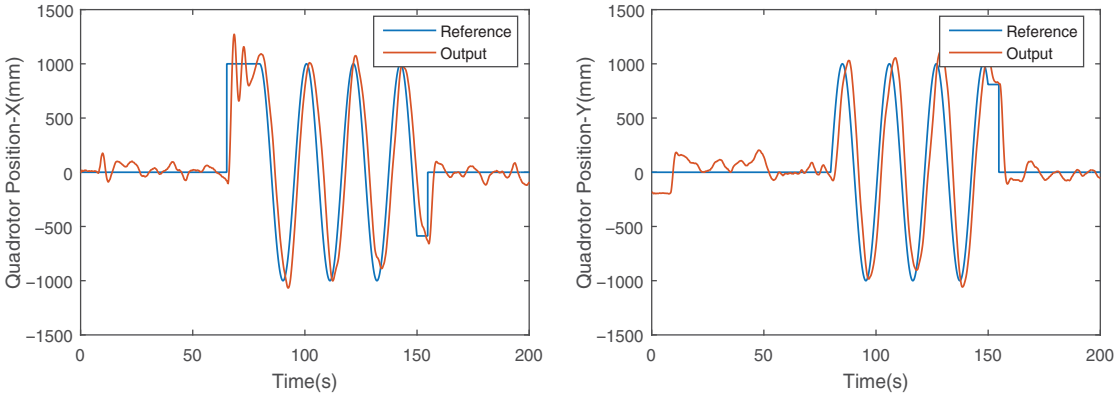

Fig. 16. Quadrotor position in experimental trajectory tracking. (a) Tracking output in X-axis. (b) Tracking output in Y-axis.

real system dynamics 100% accurate and does not have an unknown transmission delay. Additionally, the real experimental environment is much more complex than that on the Simmechanics platform. We realized the balancing by the LQR control in the simulation but we have not succeeded in the experimental system. A little change in the parameters adjustment could lead to a deadly crash sometimes. So it is worth noting that the proposed approach has a better robustness in tuning the control parameters.

5. Conclusion

In this paper, a cascade linear ADRC controller is proposed for controlling a flying inverted pendulum. After an analysis of system dynamics, a cascade controller with three loops is designed: an inner loop for onboard attitude control, a middle loop for pendulum position control and an outer loop for quadrotor position control. Both the middle and the outer loops are running on an off-board computer. Since the inverted pendulum is very sensitive to changes in quadrotor attitude, a time-scale control scheme is deployed, which involves linear feedback for the fastest inner loop, the desired attitude generation from the middle pendulum loop and the desired pendulum position generation from the slowest trajectory tracking of the outer loop.

Since the control input gain b influences system performance obviously, a changing gain design from the dynamic equations is adopted to make the observer work more efficiently instead of a traditional constant gain. Based on the performance comparison between the proposed approach and

https://doi.org/10.1017/S0263574716000035 Published online by Cambridge University Press

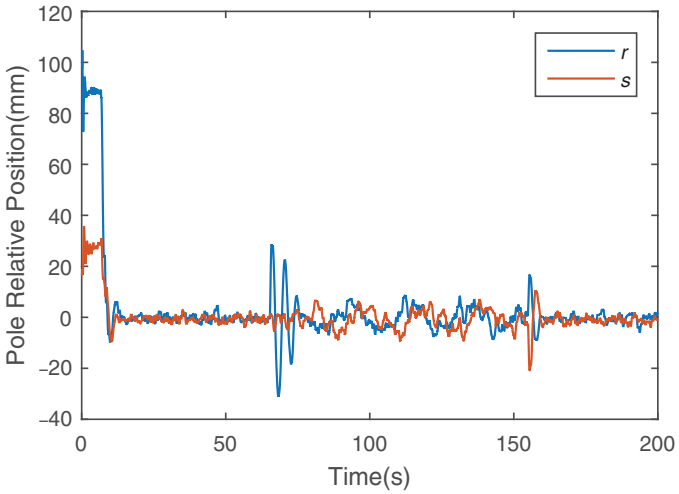

Fig. 17. Pendulum relative position in experimental trajectory tracking.

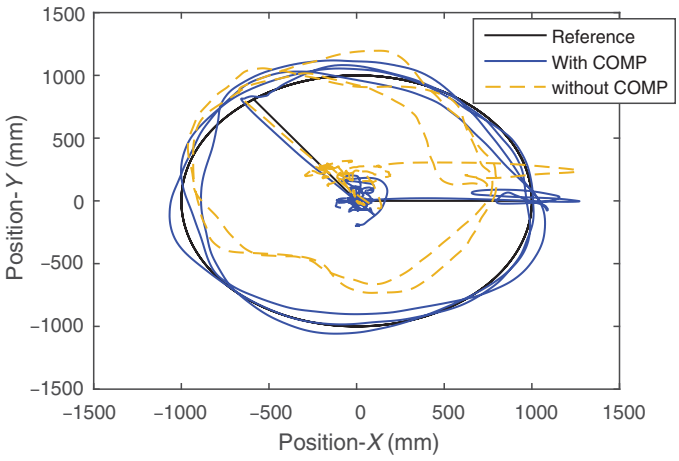

Fig. 18. Trajectory comparison between time-delay compensated and uncompensated.

an LQR controller, it is clear that the proposed method can effectively utilize the system dynamics and make a better balance between two control objectives. Therefore, the trajectory tracking is easily realized and works well under strong disturbances without further tuning.

Simulations were conducted by using the Matlab Simmechanics platform, which offers a 3D animation interface for the visualization of the system dynamics. Then, the proposed control strategy was successfully implemented on a Humming bird quadrotor in our robotics lab. To handle the time-delay caused by communications, a compensation algorithm based on a TD is added between output measurement and state observer to predict the real-time output. The experimental flight results show that the controller has fast response and excellent robustness in the face of external disturbances.

It is also worth noting that this cascade controller can be easily expanded to other under-actuated robotics systems such as aircraft and stand-up robots since it does not depend on an accurate system model. Both the simulation results and the experimental flights can be clearly watched in the videos. Our future research work includes smooth trajectory generation as well as some formation control applications.

Acknowledgments

The first author has been financially supported by China Scholarship Council. The authors would like to thank Mr. Robin Dowling and Mr. Ian Dukes at the University of Essex for their technical support.

https://doi.org/10.1017/S0263574716000035 Published online by Cambridge University Press

References

1. O. Boubaker, "The inverted pendulum benchmark in nonlinear control theory: a survey," *Int. J. Adv. Robot. Sy.* **10**, 233–242 (2013).
2. F. Grasser, A. D'Arrigo, S. Colombi and A. C. Rufer, "Joe: A mobile, inverted pendulum," *IEEE Trans. Indust. Electron.* **49**(1), 107–114 (2002).
3. J.-J. Wang, "Simulation studies of inverted pendulum based on PID controllers," *Simul. Modelling Pract. Theory* **19**(1), 440–449 (2011).
4. S. Jung, H.-T. Cho and T. C. Hsia, "Neural network control for position tracking of a two-axis inverted pendulum system: Experimental studies," *IEEE Trans. Neural Netw.* **18**(4), 1042–1048 (2007).
5. A. M. Bloch, N. E. Leonard and J. E. Marsden, "Controlled lagrangians and the stabilization of mechanical systems. I. The first matching theorem," *IEEE Trans. Autom.Control* **45**(12), 2253–2270 (2000).
6. G. Cai, J. Dias and L. Seneviratne, "A survey of small-scale unmanned aerial vehicles: Recent advances and future development trends," *Unmanned Syst.* **2**(02), 175–199 (2014).
7. J. P. How, C. Fraser, K. C. Kulling, L. F. Bertuccelli, O. Toupet, L. Brunet, A. Bachrach and N. Roy, "Increasing autonomy of uavs," *Robot. Autom. Mag. IEEE* **16**(2), 43–51 (2009).
8. S. Lupashin, M. Hehn, M. W. Mueller, A. P. Schoellig, M. Sherback and R. DAndrea, "A platform for aerial robotics research and demonstration: The flying machine arena," *Mechatronics* **24**(1), 41–54 (2014).
9. N. Michael, D. Mellinger, Q. Lindsey and V. Kumar, "The grasp multiple micro-uav testbed," *Robot. Autom. Mag. IEEE* **17**(3), 56–65 (2010).
10. M. Hehn and R. D'Andrea, "A Flying Inverted Pendulum," *Proceedings of the IEEE International Conference on Robotics and Automation (ICRA)*, Shanghai, China (2011) pp. 763–770.
11. R. Figueroa, A. Faust, P. Cruz, L. Tapia and R. Fierro, "Reinforcement Learning for Balancing a Flying Inverted Pendulum," *Proceedings of the 11th World Congress on Intelligent Control and Automation*, IEEE. Shenyang, China (2014) pp. 1787–1793.
12. C. Raimundez, J. L. Camano and A. Barreiro, "Stabilizing an Inverted Spherical Pendulum using a Scale Quad-Rotor," *Proceedings of the IEEE 4th Annual International Conference on Cyber Technology in Automation, Control and Intelligent Systems (CYBER)*, Hong Kong, China (2014) pp. 111–116.
13. J. Sandoval, R. Kelly and V. Santibanez, "On the Controlled Lagrangian of an Inverted Pendulum on a Force-Driven Cart," *Proceedings of the Control Conference (ECC), 2015 European*, IEEE. Linz, Austria (2015) pp. 992–997.
14. A. Abdessameud, I. Polushin and A. Tayebi, "Motion coordination of thrust-propelled underactuated vehicles with intermittent and delayed communications," *Syst. Control Lett.* **79**, 15–22 (2015).
15. L. Guo and S. Cao, "Anti-disturbance control theory for systems with multiple disturbances: A survey," *ISA Trans.* **53**(4), 846–849 (2014).
16. K. Ohishi, M. Nakao, K. Ohnishi and K. Miyachi, "Microprocessor-controlled dc motor for load-insensitive position servo system," *IEEE Trans. Indust. Electron.* **1**(IE-34), 44–49 (1987).
17. S. Li and J. Yang, "Robust autopilot design for bank-to-turn missiles using disturbance observers," *IEEE Trans. Aerosp. Electron. Syst.* **49**(1), 558–579 (2013).
18. D. Xing, J. Su, Y. Liu and J. Zhong, "Robust approach for humanoid joint control based on a disturbance observer," *Control Theory Appl. IET* **5**(14), 1630–1636 (2011).
19. K. K. Tan, T. H. Lee, H. F. Dou, S. J. Chin and S. Zhao, "Precision motion control with disturbance observer for pulsewidth-modulated-driven permanent-magnet linear motors," *IEEE Trans. Magn.* **39**(3), 1813–1818 (2003).
20. J. Han, "From PID to active disturbance rejection control," *IEEE Trans. Indust. Electron.* **56**(3), 900–906 (2009).
21. M. Ramirez-Neria, H. Sira-Ramirez, R. Garrido-Moctezuma and A. Luviano-Juárez, "Linear active disturbance rejection control of underactuated systems: The case of the furuta pendulum," *ISA Trans.* **53**(4), 920–928 (2014).
22. C. Zhang and J. Zhu, "On Stabilization and Disturbance Rejection for the Inverted Pendulum," *Proceedings of the IEEE International Conference on Systems, Man and Cybernetics (SMC)*, San Diego, CA (2014) pp. 3750–3754.
23. S. Esteban, F. Gordillo and J. Aracil, "Three-time scale singular perturbation control and stability analysis for an autonomous helicopter on a platform," *Int. J. Robust Nonlinear Control* **23**(12), 1360–1392 (2013).
24. G. D. Wood and D. C. Kennedy, "Simulating mechanical systems in simulink with simmechanics," Technical Report 91124v00, *The Mathworks Report Inc.*, Natick, MA, (2003).
25. D. Gurdan, J. Stumpf, M. Achtelik, K.-M. Doth, G. Hirzinger and D. Rus, "Energy-Efficient Autonomous Four-Rotor Flying Robot Controlled at 1 KHz," *Proceedings of the IEEE International Conference on Robotics and Automation*, Roma, Italy (2007) pp. 361–366.
26. F. Kendoul, "Survey of advances in guidance, navigation and control of unmanned rotorcraft systems," *J. Field Robot.* **29**(2), 315–378 (2012).
27. Z. Gao, "Scaling and Bandwidth-Parameterization Based Controller Tuning," *Proceedings of the American Control Conference*, vol. 6 Denver, Colorado, USA (2006) pp. 4989–4996.
28. I. Sa and P. Corke, "System Identification, Estimation and Control for a Cost Effective Open-Source Quadcopter," *Proceedings of the IEEE International Conference on Robotics and Automation (ICRA)*, Saint Paul, MN, USA (2012) pp. 2202–2209.
29. A. N. K. Nasir, M. A. Ahmad and M. F. Rahmat, "Performance Comparison between LQR and PID Controllers for an Inverted Pendulum System," *Proceedings of the International Conference on Power Control and Optimization: Innovation in Power Control for Optimal Industry*, AIP Publishing, vol. 1052 Chiangmai, Thailand (2008) pp. 124–128.

https://doi.org/10.1017/S0263574716000035 Published online by Cambridge University Press